Published in final edited form as:
Phys Med Biol. 2014 May 7; 59(9): N37–N48. doi:10.1088/0031-9155/59/9/N37.

Dose and detectability improvements with high energy phase sensitive x-ray imaging in comparison to low energy conventional imaging

Molly Donovan Wong, Ph.D.[1], **Aimin Yan, Ph.D.**[2], **Muhammad Ghani**[1], **Yuhua Li, Ph.D.**[1], **Laurie Fajardo, M.D.**[3], **Xizeng Wu, Ph.D.**[2], and **Hong Liu, Ph.D.**[1]

[1]University of Oklahoma Center for Bioengineering and School of Electrical and Computer Engineering 110 West Boyd Street Devon Energy Hall 150 Norman, Oklahoma 73019

[2]University of Alabama at Birmingham Department of Radiology 619 19th Street S Birmingham, Alabama 35249

[3]University of Iowa Department of Radiology 200 Hawkins Drive Iowa City, IA 52242

Abstract

The objective of this study was to demonstrate the potential benefits of using high energy x-rays for phase sensitive breast imaging through a comparison with conventional mammography imaging. We compared images of a contrast-detail (CD) phantom acquired on a prototype phase sensitive x-ray imaging system with images acquired on a commercial flat panel digital mammography unit. The phase contrast images were acquired using a micro-focus x-ray source with a 50 μm focal spot at 120 kVp and 4.5 mAs, with a magnification factor of 2.46 and a 50 μm pixel pitch. A phase attenuation duality (PAD)-based phase retrieval algorithm that requires only a single phase contrast image was applied. Conventional digital mammography images were acquired at 27 kVp, 131 mAs and 28 kVp, 54 mAs. For the same radiation dose, both the observer study and SNR/FOM comparisons indicated a large improvement by the phase retrieved image as compared to the clinical system for the larger disk sizes, but the improvement was not enough to detect the smallest disks. Compared to the double dose image acquired with the clinical system, the observer study also indicated that the phase retrieved image provided improved detection capabilities for all disk sizes except the smallest disks. Thus the SNR improvement provided by phase contrast imaging is not yet enough to offset the noise reduction provided by the clinical system at the doubled dose level. However, the potential demonstrated by this study for high energy phase sensitive x-ray imaging to improve lesion detection and reduce radiation dose in mammography warrants further investigation of this technique.

Keywords

phase sensitive; phase contrast; x-ray imaging; high energy; contrast-detail

liu@ou.edu 405.325.4286 xwu@uabmc.edu 205.934.0072

1. Introduction

Phase sensitive x-ray imaging is an active area of research with significant potential for clinical applications. Numerous studies have reported an improvement in image quality[1-14] as well as the ability to maintain the image quality with reduced radiation dose,[1-2, 5-6, 8-11] which is of critical importance in mammography due to the radio-sensitivity of the breast. However, the emerging technology faces two challenges in clinical implementation. The first relates to achieving adequate x-ray transverse coherence while providing sufficient photon flux with a polychromatic x-ray tube. While micro-focus x-ray tubes operated with large source-object distances can provide relatively large transverse coherent lengths, [15-17] a very long exposure time is required for imaging due to the limited micro-focus tube current. Secondly, although the interfaces between boundaries of different tissue areas are greatly accentuated in a phase contrast image, the bulk of the phase contrast in a given tissue area may be lost if the phase shifts vary slowly. This occurs because phase contrast is proportional to the Laplacian and gradient differentials of the phase shifts. In order to fully exhibit tissue phase contrast, one needs to disentangle tissue phase shifts from the combined attenuation/phase contrast in a phase sensitive projection. The procedure of retrieving phase shift maps from a phase sensitive projection is called phase retrieval.[18-24] The commonly used approaches require the acquisition of multiple images with varying object-detector distances per angular projection,[18-19, 22-24] which increase both the time required for image acquisition and the radiation dose to the breast. Hence, the second challenge entails developing an efficient, robust and low-dose approach to performing phase retrieval.

We have developed a new technique to overcome both of these challenges. To address the first, a micro-focus tube operating at a high tube voltage of approximately 120 kVp was used to acquire phase contrast images of a soft tissue-equivalent contrast-detail (CD) phantom. Increasing the tube voltage to 120 kVp significantly reduces the required exposure time as well as the x-ray dose per projection, due to the fact that the tube radiation output increases with at least the square of the tube voltage, and also because high energy x-rays are much more penetrating. To address the second challenge, we implemented an effective and radiation dose efficient phase retrieval approach, which is explained below.

In this study, we report results comparing CD phantom images acquired by the low energy conventional mammography technique with images acquired by our high energy phase sensitive technique. To the best of our knowledge, a comparison of relative detectability and radiation dose between clinical mammography imaging and high energy phase sensitive imaging has not been presented previously.

2. Materials and methods

2.1. Conventional x-ray imaging system configuration

The conventional mammography system utilized for this study was a GE Senographe DS flat panel digital mammography system (GE Medical, United Kingdom) with a 19 × 23 cm columnar cesium iodide (CsI) scintillator coupled to an amorphous silicon photodiode array. The system has a pixel pitch of 100 um, dual x-ray tube targets of Molybdenum and Rhodium, and 100 mA tube current with the large focal spot of 0.3 mm. Two protocols were

used to acquire conventional images, both of which utilized a source to object distance of 59.8 cm and automatic standard exposure techniques using an anti-scatter grid. The first automatic mode (Standard mode) employed settings of 28 kVp and 54 mAs with a Mo/Rh target/filter, which correspond to a half value layer (HVL) of 0.428 mm Al. The x-ray settings for the second automatic mode (Contrast mode) were 27 kVp and 131 mAs with a Mo/Rh target/filter, which correspond to a HVL of 0.418 mm Al.

2.2. Phase contrast x-ray imaging system configuration

The inline phase contrast x-ray imaging system prototype has imaging and measurement components mounted on an optical rail, which allows precise laser alignment of the x-ray source with respect to the phantom and the detector.[25] The optical rail track also provides the ability to adjust the x-ray source-to-object (*R1*) and object-to-detector (*R2*) distances to deliver a desired magnification factor: $M = (R1 + R2) / R1$.[26-27] The magnification factor for this study was selected based on the optimal phase contrast visibility, as detailed in previous studies.[12-14] The source to detector distance (*R1*+*R2*) utilized in our study was 168.91 cm, and the source to object distance (*R1*) was 68.58 cm. Thus the magnification used in the study was 2.46.

The microfocus x-ray source (Model L8121-03, Hamamatsu Photonics, Japan) utilized in this study consists of a tungsten target and a 200 μm thick Beryllium output window with adjustable tube current and voltage ranging from 40 to 150 kilovolts. The tube allows selection of the nominal focal spot size between small (7 μm), medium (20 μm) and large (50 μm) for tube operation at an output power of 10 W, 30 W and 75 W, respectively. The phase contrast images in this study were acquired with a tube voltage of 120 kVp, a tube current of 500 μA, and an exposure time of 9 sec, utilizing the large focal spot size. A 2.5 mm aluminum (Al) filter was utilized to harden the beam and block the low energy photons, as detailed in a previous study.[28] Our prototype system incorporates a CMOS flat panel sensor system (Hamamatsu C7942SK-25) with a pixel pitch of 50 μm, an active area of 120 mm × 120 mm, a frame rate of 2 fps and 12 bit digital output.

2.3. Phase retrieval

In order to fully exhibit the disk phase-contrast in the CD phantom, the phase map of the phantom must be retrieved from its phase sensitive projections. The general phase retrieval method is based on direct inversion of the x-ray propagation equation, specifically, the Transport of Intensity Equation (TIE).[18-19, 29] This requires acquisition of multiple high-dose thus low-noise projections with varying object-detector distances to retrieve the phase map, which increases the radiation dose and complicates the acquisition process. In this study, the x-ray attenuation by the CD phantom is dominated by incoherent x-ray scattering due to the use of high energy x-rays. This physical situation enables us to apply a recently developed innovative phase retrieval method known as the phase attenuation duality (PAD) method,[21-22] which requires only a single low-dose phase contrast projection image to retrieve the phase map of the phantom.

With this method, the phase map can be retrieved from just a single phase-sensitive projection $I(\vec{r}_D)$:[21-22]

$$\varphi(\vec{r}) = \frac{\lambda r_e}{\sigma_{KN}} ln\left\{\left[1 - \left(\left(\lambda^2/\sigma_{KN}\right) R_2 r_e \nabla^2/2\pi M\right)\right]^{-1} \cdot \left(M^2 I(\vec{r}_D)/I_{IN}\right)\right\}, \quad (1)$$

where $\varphi(\vec{r})$ denotes the phantom's phase map, λ is the average x-ray wavelength, σ_{KN} is the Klein-Nishina total cross-section of Compton scattering, and $r_e = 2.818 \times 10^{-15}$ m is the classical electron radius. In addition, $R_2$is the phantom-detector distance, M is the magnification factor of the projection, $\vec{r}_D$ denotes the position in the detector plane, $I(\vec{r}_D)$ is the acquired phase-sensitive projection image of the phantom, and I_{IN} is the entrance x-ray intensity. Derived from x-ray propagation equations, the operator ∇^2 in Eq. (1) denotes the two-dimensional transverse Laplacian differential operator, and the operator $\left[1 - \left(\left(\lambda^2/\sigma_{KN}\right) R_2 r_e \nabla^2/2\pi M\right)\right]^{-1}$ is a pseudo-differential operator. Due to the use of polychromatic xrays, it was necessary to approximate the values utilized in Eq. (1) for the average wavelength λ and the Klein-Nishina total cross-section σ_{KN} as those corresponding to a 60 keV x-ray, which is the approximate average output x-ray energy from a tungsten target tube operating at 120 kVp. These approximations can produce errors in the retrieved phase values, although σ_{KN} varies slowly for high energy x-rays and changes only 2.7% from 60 keV to 70 keV. Further improvement in the accuracy of phase retrieval with polychromatic x-ray sources is a topic of ongoing research that is beyond the scope of this study.

2.4. CD phantom and observer study

A CD phantom[26-27] was utilized in this study in an effort to provide a comprehensive image quality evaluation and comparison of the two systems. CD analysis is widely accepted as a simple and effective method for comparison of medical imaging systems and techniques[30-39] including mammography applications.[32, 36-39] The CD phantom (MedOptics Corporation, Tucson, Arizona) was a 4.5-cm thick acrylic phantom consisting of a 7 × 7 matrix of holes with milled depths ranging from 0.73 mm to 0.06 mm and diameters ranging from 4.82 mm to 0.18 mm. The comparison images were randomly presented to 21 independent observers for analysis, which involves each observer identifying the minimum perceptible thickness for each diameter in the image. Contrast-detail curves were generated for each image according to the averaged observers' scores to compare the relative performance of the phase retrieval and conventional clinical images. The c-d curve relates the threshold contrast necessary to perceive an object as a function of the object's diameter. Curves for different systems or techniques can easily be compared, as a system exhibiting higher performance produces a contrast-detail curve located closer to the x-y axis. A Student *t* confidence interval was constructed around each data point for the purpose of determining the variance among the observers for that point. The Student *t* distribution is frequently utilized in research environments, due to its proven ability to construct accurate confidence intervals on smaller data sets with unknown variance.[40-42] This study utilized a 95% confidence interval with $n - 1$ degrees of freedom, where n represents the number of observers.

2.5. Signal-to-noise ratio (SNR) and figure of merit (FOM) evaluations

In order to quantitatively compare the two different imaging techniques, the signal-to-noise ratios (SNRs) of the disk targets in the phantom were calculated. According to Rose, the SNR of a disk target is defined as follows:[27, 43-44]

$$SNR = \frac{S - S_B}{\sqrt{\left(\sigma^2 + \sigma_B^2\right)/2}} \times \sqrt{a_D / a_p} \quad (2)$$

where S denotes the mean pixel value of the disk target averaged over a region of interest (ROI), S_B is the mean pixel value of the background averaged over an ROI of the same size, σ^2 and σ_B^2 are the corresponding pixel value variances, and a_D and a_p are the areas of a disk target and a pixel, respectively. The achieved SNR for a given disk also depends on the radiation dose. Hence, we define a figure of merit (FOM) for target disk imaging performance, which is represented by: $FOM = SNR^2 / Dose$. The average glandular dose (D_g) is calculated as follows: $D_g = D_{gN} \cdot X_{ESE}$,[26, 45-46] where D_{gN} is the normalized average glandular dose coefficient and X_{ESE} is the object entrance exposure. D_{gN} is determined by experimental and computer simulation methods based on the following factors: radiation beam quality (x-ray energy or half value layer (HVL)), x-ray tube target material, filter material, breast thickness and breast tissue composition.[26] The D_{gN} values were determined for the conventional images from the ACR Mammography Quality Control Manual dose tables[47], which were derived from a Monte Carlo method.[39] For the phase sensitive images, D_{gN} was estimated based on the previously-described Monte Carlo method as well.[46, 48-49] However, the previous studies only provide D_{gN} data for x-ray energies up to 35 keV. To facilitate D_{gN} calculation for higher energies, we extended the Monte Carlo simulation to 150 keV. For the 120 kVp beam utilized in this study, the D_{gN} values were computed from the x-ray spectral average of the Monte Carlo simulation-derived values for various photon energies. The x-ray spectrum was measured with an x-ray spectrometer having a 3×3×1 mm^3 CdTe detector (Amptek Incorporated, Bedford, Massachusetts), using a pair of tungsten collimators provided by the manufacturer. The HVL derived from the measured spectrum was verified to match the directly measured HVL. For the conventional mammography images, the object entrance exposures and beam HVL values were measured with a newly calibrated ionization chamber and dosimeter (10X5-6M-3 chamber and Model 9010 dosimeter, Radcal Corporation, Monrovia, California). For the phase sensitive images, the measurements were obtained with a calibrated ionization chamber and dosimeter (10X9-180 chamber and Model 9095 dosimeter, Radcal Corporation, Monrovia, California). Three measurements at each mode were acquired to reduce measurement error.

3. Results and discussion

3.1. Glandular dose calculation

First, the glandular doses corresponding to the phase sensitive and conventional techniques were calculated as detailed above. The measured X_{ESE} values, the estimated D_{gN} values, and the resultant D_g values for the three imaging modes are provided in Table 1. Note that the

glandular dose values facilitate comparisons of phase contrast imaging to conventional imaging not only at similar doses but also at a reduced dose of approximately half.

3.2. Contrast-detail images

Figure 1 provides the phase-retrieved image of the CD phantom acquired at 120 kVp, 500 uA and 9 s (4.5 mAs) with a magnification factor of 2.46. Due to the limited size of the CMOS detector and the magnification factor utilized, only six of the seven test disks along each row of the CD phantom were captured on the image. No image processing methods were applied to the phase sensitive image, with the exception of window/leveling, flat field correction and dark current correction.

Figure 2 provides images of the CD phantom acquired on the clinical GE digital mammography system at 28 kVp and 54 mAs. Figure 2 (a) is the unprocessed image that has only been adjusted by window/leveling and flat field/bad pixel correction, and the processed image provided by the vendor proprietary software is given in Figure 2 (b). Similarly, Figures 3 (a) and (b) demonstrate the unprocessed and the system-processed images of the phantom acquired on the GE system at 27 kVp and 131 mAs. It should be noted that the edge enhancement applied by the clinical machine to the processed images produces a non-uniform appearance between the center and the edge of the phantom in the image, and also affects the appearance of the test targets near the edge of the phantom. In addition, this edge enhancement processing improves the detection of the disks in the image, most notably the smallest disks, which is evident when comparing the unprocessed and processed images for each dose level.

Comparing the images in Figures 1-3, for the same radiation dose, there is a large improvement in disk detection with the phase retrieved image as compared to the clinical system for the larger disk sizes, but the improvement was not enough to detect the smallest disks. Compared to the double dose image acquired with the clinical system, the observer study also indicated that the phase retrieved image provided improved detection capabilities for all disk sizes except the smallest disks. Thus the SNR improvement provided by phase contrast imaging is not yet enough to offset the noise reduction provided by the clinical system at the doubled dose level. A more detailed comparison is provided in the following sections.

3.3. Contrast-detail observer study

Figure 4 compares the contrast threshold detection performance of the phase-retrieved image with the conventional unprocessed and processed images at the tested dose level of 1.2 mGy, which is a similar dose to the phase retrieved image. For all disk sizes, the phase retrieval image is superior to the unprocessed image from the mammography system. This is a fair comparison, considering the lack of GE's proprietary image processing applied to the phase retrieved image for further enhancement. As compared to the processed GE image, the phase retrieved image exhibits improved performance for all disk sizes except the fifth row disks, where it seems that the image processing applied by the clinical system outperforms the phase retrieval imaging. For a reduced dose comparison, Figure 5 provides the contrast threshold detection performance of the phase-retrieved image with conventional GE images

at the tested dose level of 2.53 mGy, which is almost double the dose of the phase retrieved image. As compared to the clinical images, the phase retrieved image demonstrates improved detection for all but the smallest two disks. This indicates that the SNR improvement achieved with the phase imaging technique is not quite enough to offset the noise reduction capabilities provided by the clinical system at double the dose. In addition, this exhibits the operation of the phase retrieval algorithm as a low pass filter, due to the fact that it is an inverse process of phase contrast imaging. This is evidenced by the noise reduction and SNR improvement for larger objects in the phase retrieved image, but reduced detection of smaller objects, which is in part a result of the removal of the phase contrast edge enhancement through the phase retrieval.

3.4. SNR and FOM calculations

For further quantitative comparison of the two imaging techniques, we measured the Rose SNR values using Equation (2), and calculated the FOM values for four target disks in the phantom as well. The disks utilized were 3.50 mm and 4.82 mm in diameter with milled depths of both 0.73 mm and 0.51 mm for both. The unprocessed image given in Figure 2 (a) for the conventional mode with 28 kVp, 54 mAs and 1.2 mGy was utilized to compare phase sensitive with conventional images acquired at a similar dose. The unprocessed image was utilized instead of the processed image to provide a fair comparison to the phase retrieved image. In addition, the processed image could not be linearized for calculation of the SNR, due to the fact that the processing algorithm utilized by the GE clinical machine is proprietary. The results provided in Table 2 demonstrate that the SNR values calculated for the phase images range from a factor of 3 to 4.6 greater than the SNR values for the digital mammography technique for the four target-disks. Similarly, the FOM values calculated for the phase images range from a factor of 8.2 to 19.4 greater than the FOM values for the digital mammography images. These results are corroborated by the improved detection capabilities demonstrated by the phase retrieved image in the observer study comparison of the larger disk sizes. Unfortunately, as the disk detection threshold SNR increases inversely with disk size, the phase generated SNR-enhancements are not enough for the detection of smallest disks.

4. Conclusion

This study demonstrates the potential benefits of using high energy x-rays for phase sensitive breast imaging. For the same radiation dose, both the observer study and SNR/FOM comparisons indicated a large SNR improvement by the phase retrieved image as compared to the clinical system for the larger disk sizes, but the improvement was not enough to detect the smallest disks. For a reduced radiation dose, the observer study also indicated that the phase retrieved image provided improved detection capabilities for all disk sizes except the smallest disks. Thus the SNR improvement provided by phase contrast imaging is not yet enough to offset the noise reduction provided by the clinical system at double the dose. However, the potential demonstrated by this study for high energy phase sensitive x-ray imaging to improve lesion detection and reduce radiation dose in mammography warrants further investigation of this technique. Future studies will utilize

several phantoms, including those representing more complex anatomy of the breast, as well as seek to improve SNR capabilities for smaller object detection.

Acknowledgments

This research was supported in part by the NIH under grant R01CA142587, and supported in part by a grant from the University of Oklahoma Charles and Peggy Stephenson Cancer Center funded by the Oklahoma Tobacco Settlement Endowment Trust. We would like to acknowledge the support of Charles and Jean Smith Chair endowment fund as well. Xizeng Wu and Hong Liu are both considered corresponding authors.

REFERENCES

1. Arfelli F, Assante M, Bonvicini V, Bravin A, Cantatore G, Castelli E, Dalla Palma L, Di Michiel M, Longo R, Olivo A, Pani S, Pontoni D, Poropat P, Prest M, Rashevsky A, Tromba G, Vacchi A, Vallazza E, Zanconati F. Low-dose phase contrast x-ray medical imaging. Physics in Medicine and Biology. 1998; 43(10):2845–2852. [PubMed: 9814522]
2. Donnelly E, Price R, Pickens D. Quantification of the effect of system and object parameters on edge enhancement in phase-contrast radiography. Medical Physics. 2003; 30(11):2888–2896. [PubMed: 14655935]
3. Freedman M, Lo S, Honda C, Makariou E, Sisney G, Pien E, Ohara H, Ishisaka A, Shimada F. Phase contrast digital mammography using molybdenum x-ray: clinical implications in detectability improvement. SPIE. 2003; 5030:533–540.
4. Ingal V. Phase mammography-a new technique for breast investigation. Physics in Medicine and Biology. 1998; 43:2555–2567. [PubMed: 9755945]
5. Kotre C, Birch I. Phase contrast enhancement of x-ray mammography: a design study. Physics in Medicine and Biology. 1999; 44:2853–2866. [PubMed: 10588289]
6. Matsuo S, Katafuchi T, Tohyama K, Morishita J, Yamada K, Fujita H. Evaluation of edge effect due to phase contrast imaging for mammography. Medical Physics. 2005; 32(8):2690–2697. [PubMed: 16193800]
7. Momose A, Fukuda J. Phase-contrast radiographs of non-stained rat cerebellar specimen. Medical Physics. 1995; 22(4):375–379. [PubMed: 7609717]
8. Pogany A, Gao D, Wilkins S. Contrast and resolution in imaging with a microfocus x-ray source. Review of Scientific Instruments. 1997; 68(7):2774–2782.
9. Tanaka T, Honda C, Matsuo S, Noma K, Oohara H, Nitta N, Ota S, Tsuchiya K, Sakashita Y, Yamada A, Yamasaki M, Furukawa A, Takahashi M, Murata K. The first trial of phase contrast imaging for digital full-field mammography using a practical molybdenum X-ray tube. Investigative Radiology. 2005; 40(7):385–396. [PubMed: 15973129]
10. Wilkins S, Gureyev T, Gao D, Pogany A, Stevenson A. Phase-contrast imaging using polychromatic hard x-rays. Nature. 1996; 384(6607):335–338.
11. Zhang D, Donovan M, Fajardo L, Archer A, Wu X, Liu H. Preliminary feasibility study of an in-line phase contrast x-ray imaging prototype. IEEE Transactions on Biomedical Engineering. 2008; 55(9):2249–2257. [PubMed: 18713694]
12. Castelli E, Tonutti M, Arfelli F, Longo R, Quaia E, Rigon L, Sanabor D, Zanconati F, Dreossi D, Abrami A, Quai E, Bregant P, Casarin K, Chenda V, Menk RH, Rokvic T, Vascotto A, Tromba G, Cova MA. Mammography with synchrotron radiation: first clinical experience with phase-detection technique. Radiology. 2011; 259(21436089):684–694. [PubMed: 21436089]
13. Quai E, Longo R, Zanconati F, Jaconelli G, Tonutti M, Abrami A, Arfelli F, Dreossi D, Tromba G, Cova MA. First application of computed radiology to mammography with synchrotron radiation. La radiologia medica. 2013; 118(1):89–100. [PubMed: 22744351]
14. Tanaka J, Nagashima M, Kido K, Hoshino Y, Kiyohara J, Makifuchi C, Nishino S, Nagatsuka S, Momose A. Cadaveric and in vivo human joint imaging based on differential phase contrast by X-ray Talbot-Lau interferometry. Zeitschrift für Medizinische Physik. 2013; 23(3):222–227. [PubMed: 23219283]

15. Wu X, Liu H. Clinical implementation of x-ray phase-contrast imaging: theoretical foundations and design considerations. Medical Physics. 2003; 30(8):2169–2179. [PubMed: 12945983]
16. Wu X, Liu H. Clarification of aspects in in-line phase-sensitive x-ray imaging. Medical Physics. 2007; 34(2):737–743. [PubMed: 17388191]
17. Wu X, Liu H. Phase-space evolution of x-ray coherence in phase-sensitive imaging. Applied Optics. 2008; 47(22):E44–E52. [PubMed: 18670541]
18. Cloetens P, Mache R, Schlenker M, Lerbs-Mache S. Quantitative phase tomography of Arabidopsis seeds reveals intercellular void network. Proceedings of the National Academy of Sciences. 2006; 103(39):14626–14630.
19. Nugent KA, Gureyev TE, Cookson DJ, Paganin D, Barnea Z. Quantitative Phase Imaging Using Hard X Rays. Physical Review Letters. 1996; 77(14):2961–2964. [PubMed: 10062096]
20. Wu X, Liu H. X-Ray cone-beam phase tomography formulas based on phase-attenuation duality. Optics Express. 2005; 13(16):6000–6014. [PubMed: 19498608]
21. Wu X, Liu H, Yan A. X-ray phase-attenuation duality and phase retrieval. Optics Letters. 2005; 30:379–381. [PubMed: 15762434]
22. Wu X, Yan A. Phase retrieval from one single phase contrast x-ray image. Optics Express. 2009; 17(13):11187–11196. [PubMed: 19550519]
23. Yan A, Wu X, Liu H. An attenuation-partition based iterative phase retrieval algorithm for in-line phase-contrast imaging. Optics Express. 2008; 16(17):13330–13341. [PubMed: 18711570]
24. Yan A, Wu X, Liu H. Performance analysis of the attenuation-partition based iterative phase retrieval algorithm for in-line phase-contrast imaging. Optics Express. 2010; 18(15):16074–16089. [PubMed: 20720992]
25. Zhang D, Wong M, Wu X, Liu H. A convenient alignment approach for x-ray imaging experiments based on laser positioning devices. Medical Physics. 2008; 35(11):4907–4910. [PubMed: 19070224]
26. Bushberg, J.; Seibert, J.; Leidholdt, E., Jr.; Boone, J. The Essential Physics of Medical Imaging. Second ed. Lippincott Williams & Wilkins; Philadephia, Pennsylvania: 2002.
27. Hasegawa, B. The Physics of Medical X-Ray Imaging. Medical Physics Publishing Corporation; Madison, Wisconsin: 1990.
28. Wong M, Wu X, Liu H. The effects of x-ray beam hardening on detective quantum efficiency and radiation dose. Journal of X-Ray Science and Technology. 2011; 19:509–519.
29. Allen LJ, Oxley MP. Phase retrieval from series of images obtained by defocus variation. Optics Communications. 2001; 199(1–4):65–75.
30. Aufrichtig R. Comparison of low contrast detectability between a digital amorphous silicon and a screen-film based imaging system for thoracic radiography. Medical Physics. 1999; 26(7):1349–1358. [PubMed: 10435537]
31. Donovan M, Zhang D, Chen W, Liu H. The characterization of a phase contrast x-ray imaging prototype. SPIE. 2007; 6436(643608):9.
32. Liu H, Fajardo L, Barrett J, Baxter R. Contrast-detail detectability analysis: comparison of a digital spot mammography system and an analog screen-film mammography system. Academic Radiology. 1997; 4(3):197–203. [PubMed: 9084777]
33. Pogue B, Willscher C, McBride T, Osterberg U, Paulsen K. Contrast-detail analysis for detection and characterization with near-infrared tomography. Medical Physics. 2000; 27(12):2693–2700. [PubMed: 11190952]
34. Rong X, Shaw C, Liu X, Lemacks M, Thompson S. Comparison of an amorphous silicon/cesium iodide flat-panel digital chest radiography system with screen/film and computed radiography systems - a contrast-detail phantom study. Medical Physics. 2001; 28(11):2328–2335. [PubMed: 11764040]
35. Zhang Q, Li Y, Steele B, Wu X, Chen W, Rong J, Liu H. Comparison of a CMOS-based and a CCD-based digital x-ray imaging system: observer studies. Journal of Electronic Imaging. 2005; 14(2):23002, 23006.
36. Berns EA, Hendrick R. Edward, Cutter Gary R. Performance comparison of full-field digital mammography to screen--film mammography in clinical practice. Medical Physics. 2002; 29(5): 830–834. [PubMed: 12033579]

37. Karellas A, Vedantham S. Breast cancer imaging: A perspective for the next decade. Medical Physics. 2008; 35(11):4878–4897. [PubMed: 19070222]
38. Robson KJ, Kotre CJ, Faulkner K. The use of a contrast–detail test object in the optimization of optical density in mammography. British Journal of Radiology. 1995; 68(807):277–282. [PubMed: 7735767]
39. Suryanarayanan S, Karellas A, Vedantham S, Ved H, Baker SP, D'Orsi CJ. Flat-Panel Digital Mammography System: Contrast-Detail Comparison between Screen-Film Radiographs and Hard-Copy Images1. Radiology. 2002; 225(3):801–807. [PubMed: 12461264]
40. Larsen, R.; Marx, M. An Introduction to Mathematical Statistics and Its Applications. Fourth ed. Pearson Prentice Hall; Upper Saddle River, NJ: 2006.
41. Mendenhall, W.; Sincich, T. Statistics for Engineering and the Sciences. 5th Edition ed. Prentice Hall; Upper Saddle River, New Jersey: 2007.
42. Papoulis, A.; Pillai, S. Probability, Random Variables and Stochastic Processes. Fourth Edition ed. McGraw-Hill; New York City, New York: 2002.
43. Rose A. The sensitivity performance of the human eye on an absolute scale. Journal of the Optical Society of America. 1948; 38:196–208. [PubMed: 18901781]
44. Liu H, Karellas A, Moore SC, Harris LJ, D"Orsi CJ. Lesion detectability considerations for an optically-coupled CCD X-ray imaging system. Nuclear Science, IEEE Transactions on. 1994; 41(4):1506–1509.
45. Boone J. Glandular Breast Dose for Monoenergetic and High-Energy X-ray Beams: Monte Carlo Assessment. Radiology. 1999; 213(1):23–37. [PubMed: 10540637]
46. Wu X, Gingold E, Barnes G, Tucker D. Normalized Average Glandular Dose in Molybdenum Target-Rhodium Filter and Rhodium Target-Rhodium Filter Mammography. Radiology. 1994; 193(1):83–89. [PubMed: 8090926]
47. Hendrick R, Bassett L, Botsco M, Butler P, Dodd G, Feig S, Gray J, Haus A, Harvey M, Heinlein R, Holland R, Kitts E Jr. McLelland R, McCrohan J, Rossi R, Sullivan D. Mammography Quality Control Manual. American College of Radiology. 1994:43–51.
48. Wu X, Barnes G, Tucker D. Spectral dependence of glandular tissue dose in screen-film mammography. Radiology. 1991; 179:143–148. [PubMed: 2006265]
49. Wu X. Breast Dosimetry in Screen Film Mammography. Screen Film Mammography: Imaging Considerations and Medical Physics Responsibilities. 1991:159–175.

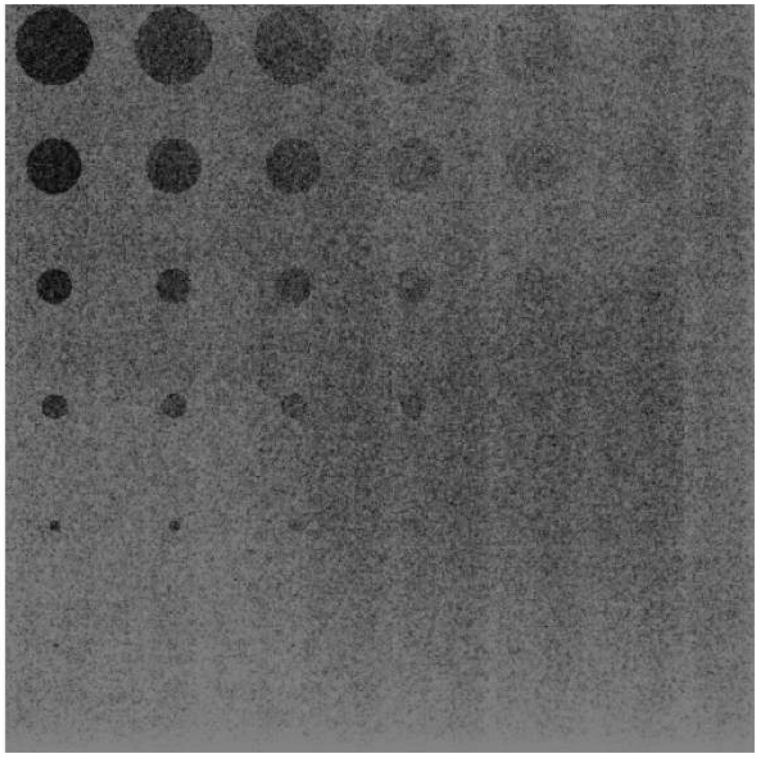

Figure 1.

Phase-retrieved image acquired at 120kVp, 500uA and 9 sec (4.5 mAs) with a magnification factor of 2.46 and an average glandular dose of 1.295 mGy.

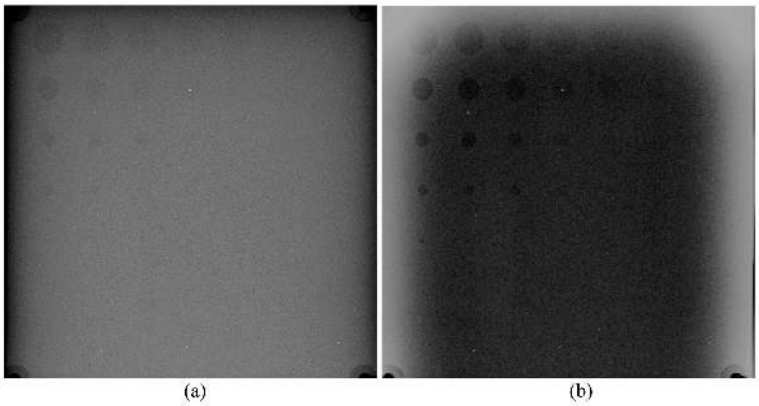

Figure 2.

Images acquired by GE mammography clinical system with 28kVp, 54 mAs at 1.2mGy: (a) the unprocessed image, and (b) the processed image displayed by the GE clinical system.

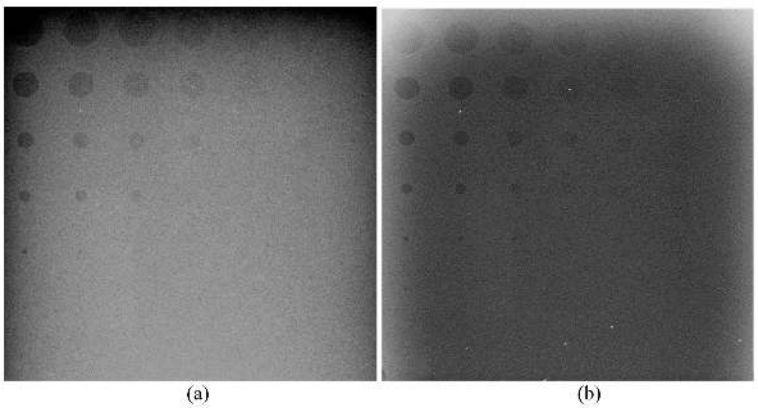

Figure 3.

Images acquired by the clinical GE mammography system with 27 kVp, 131 mAs and 2.53 mGy: (a) the unprocessed image, and (b) the processed image displayed by the GE clinical system.

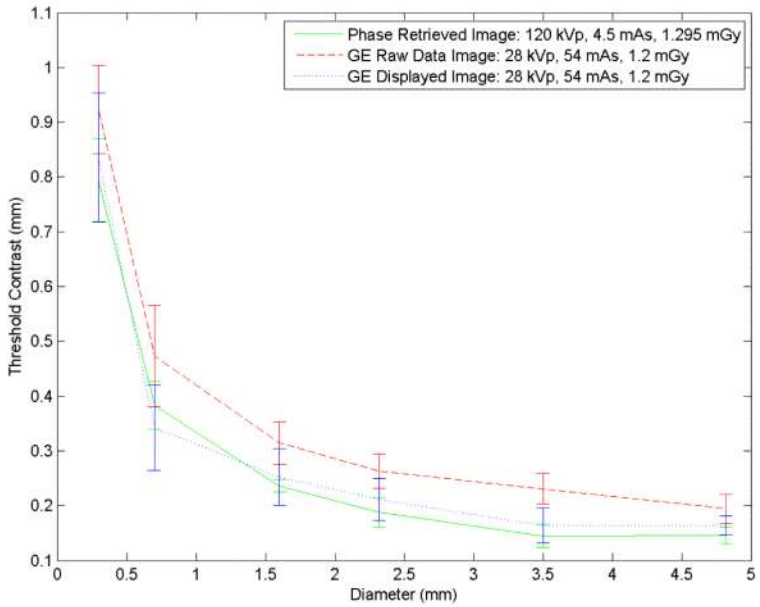

Figure 4.

Contrast-detail curve comparison of the phase-retrieved image with both the unprocessed and processed images acquired by the GE digital mammography system at a similar dose.

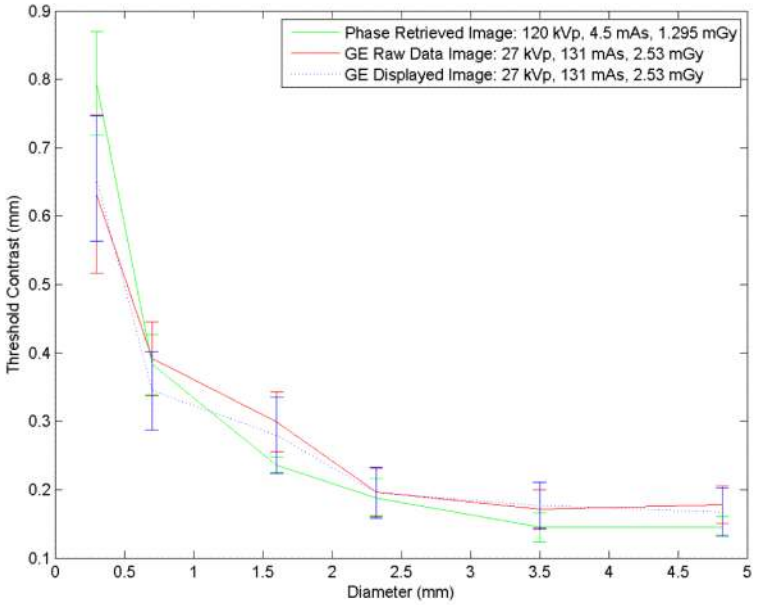

Figure 5.

Contrast-detail curve comparison of the phase retrieved image with both the unprocessed and processed images acquired by the GE digital mammography system at a doubled dose.

Table 1

Average glandular dose measurements for all techniques

	X_{ESE} (mR)	D_{gN}(mrad/R)	D_g(mGy)
Conventional Mammography: 28 kVp, 54 mAs	558.0	216	1.200
Conventional Mammography: 27 kVp, 131 mAs	1200.0	210	2.530
Phase Sensitive: 120 kVp, 4.5 mAs	191.6	676	1.295

Table 2

Comparison of the SNR and FOM ratios for the two imaging techniques with approximately the same average glandular doses: 1.295 mGy with phase sensitive imaging and 1.2 mGy with conventional mammography

	4.82-mm disk 0.73-mm deep	4.82-mm disk 0.51-mm deep	3.50-mm disk 0.73-mm deep	3.50-mm disk 0.51-mm deep
Ratio of SNR with phase sensitive imaging to mammography	3.3	3.0	4.1	4.6
Ratio of FOM with phase sensitive imaging to mammography	10.0	8.2	15.6	19.4